Characterization of metal oxide micro/nanoparticles elaborated by plasma electrolytic oxidation of aluminium and zirconium alloys

J. Martin, P. Haraux, V. Ntomprougkidis, S. Migot, S. Bruyère, G. Henrion

▶ **To cite this version:**

J. Martin, P. Haraux, V. Ntomprougkidis, S. Migot, S. Bruyère, et al.. Characterization of metal oxide micro/nanoparticles elaborated by plasma electrolytic oxidation of aluminium and zirconium alloys. Surface and Coatings Technology, 2020, 397, pp.125987. 10.1016/j.surfcoat.2020.125987 . hal-02910106

HAL Id: hal-02910106

https://hal.univ-lorraine.fr/hal-02910106

Submitted on 12 Nov 2020

HAL is a multi-disciplinary open access archive for the deposit and dissemination of scientific research documents, whether they are published or not. The documents may come from teaching and research institutions in France or abroad, or from public or private research centers.

L'archive ouverte pluridisciplinaire **HAL**, est destinée au dépôt et à la diffusion de documents scientifiques de niveau recherche, publiés ou non, émanant des établissements d'enseignement et de recherche français ou étrangers, des laboratoires publics ou privés.

Characterization of metal oxide micro/nanoparticles elaborated by plasma electrolytic oxidation of aluminium and zirconium alloys

J. Martin*, P. Haraux, V. Ntomprougkidis, S. Migot, S. Bruyère, G. Henrion

Université de Lorraine, CNRS, IJL, F-54000 Nancy, France, Campus ARTEM, 2 allée André Guinier, 54000 Nancy, France

*Corresponding author: +33 (0)3.72.74.24.97, julien.martin@univ-lorraine.fr

Highlights

- PEO process produces polycrystalline metal oxide particles (Al_2O_3 and ZrO_2)
- Particles exhibit a hollow spherical morphology with size between 0.01-10 µm
- Morphology of the particles is correlated to the PEO "pancake" structure
- A formation mechanism of particles during PEO is proposed

Graphical abstract

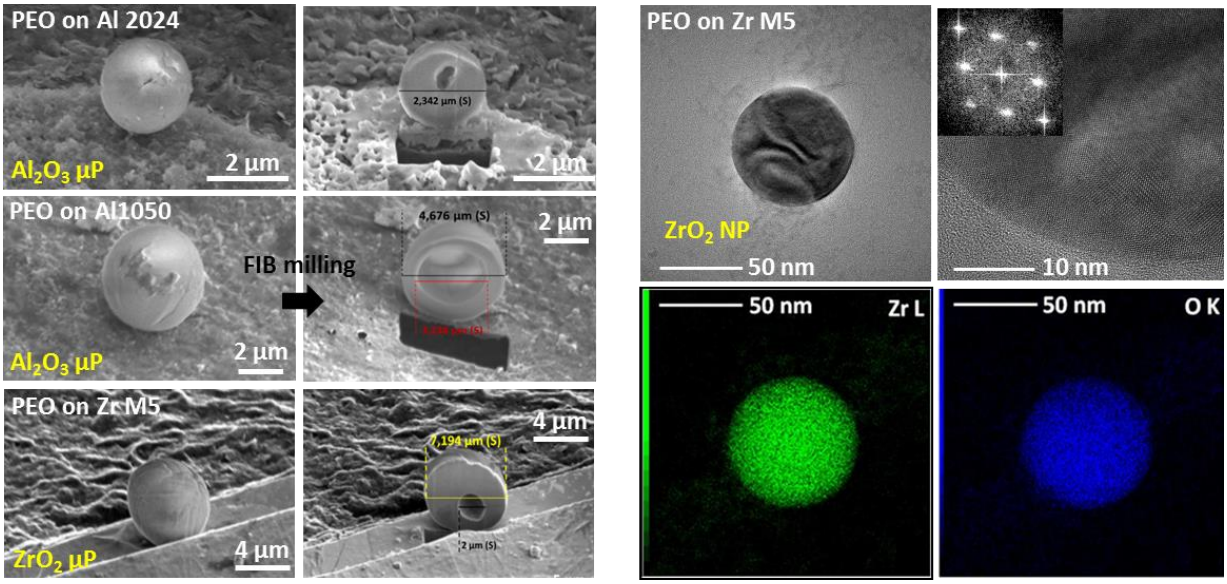

Abstract

The formation of fine particles during the Plasma Electrolytic Oxidation process (PEO) was investigated. Particles were produced by carrying out PEO treatments on two different grade of aluminium alloy (Al1050, Al2024) and a low-alloyed zirconium grade (Zr-M5). They were characterized at different scales mainly using transmission electron microscopy. Whatever the processed material, results show that particles exhibit a hollow spherical shape with outer diameter ranging from 100 nm to 10 µm. They consist of polycrystalline alumina (η- and α-Al_2O_3) for the PEO of aluminium alloys and zirconia (m-ZrO_2) for the zirconium alloy. A correlation is drawn between the microstructure of the produced particles and the "pancake"-like structure that usually develops over PEO coatings. On this basis, a descriptive mechanism of the formation of these metal oxide particles is proposed. The ignition of a micro-discharge inside the "pancake" cavity induces the propagation of a pressure shockwave that pushes the molten oxide through the narrow orifice of the "pancake" structure. Like a rubber balloon, the molten oxide forms a hollow sphere and is rapidly quenched by the surrounding electrolyte and ejected into the electrolyte.

Keywords: Plasma electrolytic oxidation (PEO); Micro-arcs oxidation (MAO); Aluminium, Zirconium; Metal oxide particles; Oxide coatings

1. Introduction

Plasma electrolytic oxidation (PEO), also referred to as micro-arc oxidation (MAO), is an anodic plasma electrolysis process that allows growing protective ceramic-like oxide coatings on valve metals such as aluminium, titanium, magnesium and zirconium alloys [1-4]. PEO process gains a growing interest in various industrial domains (transport, energy, medicine) to replace conventional chromic acid anodizing (CAA) or hard acid anodizing (HAA) [5, 6]. Indeed, PEO results in improved wear and corrosion resistance together with enhanced thermal stability and biocompatibility properties [6-8]. PEO also uses low concentrated alkaline electrolytes depleted in toxic compounds, which makes it an environmentally friendly process. Achieved at a voltage higher than the dielectric breakdown voltages of the growing oxide layer, PEO coatings are formed under an anodic sparking regime characterized by the ignition of tiny and short-lived micro-discharges that ignite randomly over the processed surface. This sparking regime gradually leads to the conversion of the processed metal into a crystalline oxide layer [9-12]. The formation mechanisms of the protective PEO coatings remain complex due to the combination of thermal-, electro-, and plasma-assisted chemical reactions that simultaneously occur in a low affected volume (tens of μm^3) [13-17].

Among the inherent aspects of the PEO process, it is frequently observed that the PEO process generates residual particles that are usually found at the bottom of the electrolytic cell. The particles produced during the PEO process have been very little studied. Zhan *et al.* [18] reported the synthesis of WO_3 particles during PEO of Al in a tungstate electrolyte. They showed that particles exhibit an irregular shape with a size distribution ranging from 100 nm to 1 µm. Authors explained their formation by the decomposition of the electrolyte species within the micro-discharge plasma. Surprisingly, they did not evidence the simultaneous formation of Al_2O_3 particles. In addition, the synthesis of particles via cathodic plasma electrolysis processes is widely documented in the literature [19-29]. During cathodic plasma electrolysis, a thin

gaseous envelope (mainly containing hydrogen) forms around the cathode; the latter is therefore separated from the surrounding electrolyte. When the applied voltage is high enough to induce the dielectric breakdown of the gaseous envelope, a quite stable glow-discharge plasma sheath is created and covers the cathode [19]. Within this cathodic plasma discharge regime, the processed metal rapidly erodes and melted particles are released from the cathode into the water-based electrolyte [20, 21]. When particles enter into the surrounding cold electrolyte, they usually solidify into spherical nanoballs with diameter ranging from 10 nm to 10 µm, depending on the operating material and the electrolyte chemistry [22-23]. When subsequently exposed to air, the surface of some particles gets oxidized, thus forming core-shell structures with attractive new properties like photocatalytic effects for instance [24-27]. Various metal or metal oxide nanoparticles have been successfully produced by cathodic plasma electrolysis including steel, copper titanium, zinc, silver, nickel, gold and platinum [21, 28, 29].

However, the mechanisms that govern the cathodic plasma electrolysis strongly differ from those encountered in PEO during which localized micro-discharges ignite at the anode due to the dielectric breakdown of the growing oxide layer [5, 13, 17]. Consequently, it is reasonable to assume that particles produced with the PEO process would exhibit microstructural differences compared to those collected during cathodic plasma electrolysis. This motivated the present study that consists in deeply investigating the microstructure of the particles formed during the PEO process. Comparatively, the microstructure of the PEO oxide layer grown within the same conditions are also characterized and compared to the produced particles. Finally, on the basis of the experimental results, a descriptive mechanism of the formation of particles during anodic plasma electrolysis is discussed.

2. Experimental procedure

2.1 Materials

The PEO processed materials consisted of three commercial metallic alloys, a low-alloyed aluminium (Al-1050 grade), a copper-rich aluminium alloy (Al-2024 grade) and a low-alloyed zirconium (Zr-M5 grade). Table 1 gives the chemical composition of these three alloys. The Al-1050 and the Al-2024 aluminium samples had a rectangular shape of 45 mm × 25 mm × 5 mm in size while the Zr-M5 zirconium samples exhibited a tubular shape of 30 mm in height, 15 mm in external diameter and 1 mm in thickness. Dimensions of all samples were chosen to keep the same surface area (0.28 dm^2), and therefore the same current density applied to the PEO-processed samples.

2.2 PEO processing conditions

The samples were PEO-processed in 4 L beaker containing a low-concentrated solution of potassium hydroxide ([KOH] = 1 $g.L^{-1}$ ≅ 0.018 $mol.L^{-1}$) diluted in deionised water. In order to prevent the electrolyte from any pollution, and to avoid the dissemination of the produced particles in the cooling circuit, the electrolyte was cooled using a double wall system. As described in Fig. 1a, the beaker containing the electrolyte is located into a larger tank filled with a stream of cold water. A magnetic stirrer at the bottom of the beaker ensures the homogenization of the electrolyte temperature. Within these cooling conditions, the electrolyte temperature was kept below 60 °C. For each PEO treatment, the processed sample was systematically located at 90 mm apart from the counter-electrodes (two titanium plates of 200 mm × 200 mm × 1 mm in size). PEO treatments were carried out using a pulsed bipolar current generator within the so-called "soft" regime electrical conditions [30-33]. Within these electrical conditions, the ratio of anodic to cathodic charge quantity ($RCQ = Q_p/Q_n$) was set at 0.9. The current pulse frequency (F), the anodic current amplitude (I_a) and the anodic current density (j_a) were set at 100 Hz, 10 A and 36 $A.dm^{-2}$, respectively. The duration of all the PEO treatments was fixed at 30 min. It is worth mentioning that, although PEO treatments were

performed in electrical conditions that would allow the "soft" regime to occur at about 50 min., the transition from the "arc" to the "soft" growth regime did not appear due to a too short processing duration [34].

2.3 Particles collection and *ex situ* characterization

As illustrated in Fig. 1b, the electrolyte containing suspended particles was then filtered using the Büchner filtering method. The filter paper used (Whatman® Cyclopore™ polycarbonate membrane) allowed retaining particles with size larger than 100 nm. Additionally, a TEM grid that consists of a 300 mesh nickel grid covered with a carbon film was also placed onto the surface of the filter paper. After filtering, the filter paper and the TEM grid were dried in an oven at 60 °C for 12 h.

Pictures of the electrolyte and the filter paper were taken before and after filtering. The particles remaining onto both the filter paper and on the TEM grid were observed using SEM and TEM techniques. Different magnifications were used in order to estimate the size distribution of the produced particles. The chemical composition and the elemental distribution of the formed particles were determined by EDX and STEM/EDX analyses. The crystallographic phase composition of the particles was investigated by XRD measurements operated in Bragg-Brentano geometry with a step size of 0.005° and a scan range from 30 to 60°. XRD measurements were performed on the surface of the filter paper using a Cu-$K_{\alpha 1}$ radiation at wavelength λ = 0.1542 nm. Observation of the high-resolution TEM images combined with the analysis of the corresponding FFT patterns also led us to determine the phase composition of the produced particles. Additionally, FIB milling technique (Focused Ion Beam using a Ga^+ beam) was also used to cut the produced particles in half and to characterize their internal morphology. Finally, for comparison reasons, PEO coatings grown on the different substrates were also characterized by SEM, EDX and XRD techniques.

3. Results

3.1 Morphology of the particles

Fig. 2 shows the visual aspect of the electrolytes and the filter papers before and after the filtering step. Whatever the processed substrate, the electrolytes are colored before filtering while they are transparent after filtering. This suggests the presence of particles. The visual aspect of the filter papers after filtering also confirms the presence of particles in the electrolyte after the PEO treatment. PEO processing of the copper-alloyed aluminum (Al-2024) results in a brown coloured filter. In contrast, the filter exhibits a whitish appearance in the case of the low-alloyed aluminum (Al-1050). For the low-alloyed zirconium, the filter paper appears pinkish-brown.

Fig. 3 shows the SEM micrographs of the filter paper before and after the filtering step in the case of the PEO process of the copper-alloyed aluminium (Al-2024). Before filtering, no particle is observed at the surface of the filter paper (Fig. 3a) while spherical particles with different sizes are observed after filtering (Fig. 3b, c, d). Fig. 4 shows the size distribution of the spherical particles observed for all the processed substrates. Whatever the processed substrate, particles exhibit quite the same size distribution, in the range of 0.1 - 10 µm, with a mean size of ~ 4 µm and the most probable size of 3 µm. Additionally, high magnification SEM micrograph in Fig. 3d show that particles are not perfectly spherical since some cracks and holes are visible over their surface. It is also worth mentioning that similar observations were done in the case of the PEO processing of Al-1050 and Zr-M5 samples.

Some of these particles were cut in half using FIB milling technique. Whatever the PEO-processed material, SEM micrographs in Fig. 5 show that particles exhibit an internal cavity that, for certain particles, opens outwards. Interestingly, the internal and the external morphology of the particles remain the same irrespective of the processed alloy. It suggests that

the formation of particles follows an inherent mechanism of the PEO process and is independent of the processed metallic alloy.

3.2 Chemical composition of the particles

The elemental composition of the produced particles was determined by using EDX method. The EDX spectra given in Fig. 6 were recorded on the particles as indicated in Fig. 5. EDX spectra recorded on the particles produced with Al-2024 and Al-1050 show that they exclusively contain Al and O elements suggesting thereby the formation of alumina particles. The particles produced with the Zr-M5 are exclusively composed of Zr and O elements suggesting in this case the formation of zirconia particles.

These first elemental analyses were confirmed by the element distributions and quantifications done with STEM/EDX analyses as shown in Fig. 7 and in Table 2, respectively. Spherical particles formed during the PEO process of the two aluminium alloys (Al-1050 and Al-2024) are mainly composed of Al and O. Their atomic concentration is close to the stoichiometry of alumina Al_2O_3 (Spot 4 and spot 6 in Table 2). The particles produced with the zirconium alloy are rich in Zr and O and their atomic concentration is close to the stoichiometry of zirconia ZrO_2 (Spot 7 in Table 2). Additionally, in the specific case of the copper-alloyed aluminium (Al-2024), bright-field micrographs evidence the presence of nanometre-size needles surrounding the Al, O-rich spherical particle. The EDX element quantification performed on these needles (Spot 5 in Table 2) reveals the presence of Cu and O in large amount suggesting that they consist of copper oxide. In contrast, no similar needle was detected in the case of the low-alloyed aluminium substrate (Al-1050). Finally, detection of carbon residues is associated to the carbon film deposited on the TEM grid while titanium traces may come from the gradual erosion of the titanium counter-electrodes during the PEO treatments.

3.3 Crystallographic phase composition of the particles

Fig. 8 shows the XRD patterns of the PEO processed alloys (Al-2024, Al-1050 and Zr-M5), the resulting PEO oxide coatings and the filter papers (after filtering the electrolyte). First, XRD patterns of the PEO layers show the presence of Al and Zr peaks in the case of the PEO process of the aluminium alloys (Al-1050 and Al-2024) and the zirconium alloy (Zr-M5), respectively. They originate from the metallic substrate lying beneath the oxide layer due to the X-ray penetration depth that exceeds the overall thickness of the formed PEO coating. Second, and as usually encountered for the PEO process of aluminium [12] and zirconium alloys [3], the XRD patterns reveal the presence of two types of alumina (face-centred cubic η- and rhombohedral α-Al_2O_3) through the PEO coatings grown on the two aluminium alloys and one type of zirconia (monoclinic ZrO_2) through the PEO layer produced on the zirconium alloy. Third, indexing the XRD patterns recorded on the filter papers only evidences the presence of η- ,α-Al_2O_3 and ZrO_2 for the PEO process of the aluminium and the zirconium alloys, respectively. In the specific case of the copper-alloyed aluminium (Al-2024), the presence of copper oxide CuO is observed. As a consequence, XRD measurements performed on the filter papers confirm the fact that the spherical particles consist of crystallized alumina or zirconia, depending on the metallic substrate, while the needle-shaped nanostructures are composed of crystallized copper oxide. The presence of CuO in the case of the copper-alloyed aluminium explains the brown-coloured electrolyte as seen in Fig. 2. The partial dissolution in the alkaline electrolyte of the Al_2Cu intermetallic compounds contained in the Al-2024 substrate can explain the formation of CuO. This results in the formation of $Cu(OH)_2$ precipitates that subsequently experiences a plasma-assisted thermal decomposition into CuO [35, 36].

These results were doubly checked by performing deeper TEM observations as shown in Fig. 9. Bright-field TEM micrographs show that nanometre-sized spherical particles are also produced. High-resolution TEM micrographs confirm the crystalline state of the produced particles. Moreover, indexing the associated FFT patterns confirm the presence of η-Al_2O_3 in

the spherical particles produced during PEO of the Al-2024 substrate. The composition of the surrounding needle shaped particles is indeed CuO. Finally, spherical particles produced from the Zr-M5 substrate are crystallized under the m-ZrO_2 phase.

4. Discussion

The discussion hereafter focuses on the formation of metal oxide particles during the PEO process. Particularly, a descriptive mechanism is proposed to explain their specific morphology *i.e.* a hollow spherical shape with cracks at their surface; this morphology is independent of the nature of the processed material. The proposed mechanism is mainly based on a close comparison between the morphology of these particles and the morphology of the corresponding elaborated PEO coatings.

Fig. 10 shows the cross-sectional and the top-surface SEM micrographs of the PEO coating elaborated on the copper-alloyed aluminium (Al-2024). The observed morphology is characteristic of PEO coatings elaborated under the "arc" sparking regime (before the appearance of the "soft" regime) with the presence of large open discharge channels forming "pancake"-like structures over the top-most surface. Moreover, the associated XRD patterns evidence the presence of two crystalline polymorphs of alumina *i.e.* α- and η-Al_2O_3. As a comparison, it was previously established that particles produced from the Al2024 alloy also consist of these two crystalline polymorphs (Fig. 8 and 9). More interestingly, a close examination of the top-surface of the coating reveals the presence of spherical particles (Fig. 10). The latter is as attached at the top-surface of the coating, particularly near the "pancake" structure. Their spherical shape is the same as that of the particles observed on the filter paper. Fig. 10 also shows that the size of the attached particle is of the same order of magnitude as the diameter of the cavity of the surrounding "pancake", in the micrometre range. Finally, the EDX spectrum recorded on this attached particle shows that it consists mainly of Al and O suggesting the presence of crystalline alumina. Thus, close similarities are drawn between the

microstructure of the produced particles and the grown PEO coating, mainly the typical morphology of the "pancake" structure. As depicted in Fig. 11, these similarities allow proposing a formation mechanism of metal oxide particles inherent to the PEO process.

As described previously with SEM observations, Fig. 11a presents the typical "pancake" structure that develops during the PEO within the "arc" regime. Nominé *et al.* have demonstrated that micro-discharges appear in "cascade" through the discharge channel of a "pancake" structure [37, 38]. From optical emission spectroscopy measurements, Martin *et al.* recently estimated the gas temperature in the micro-discharge at about 3200 K [12]. At this temperature, the pre-formed oxide layer is locally and rapidly melted at a heating rate of ~10^8 $K.s^{-1}$ (Fig. 11b). Troughton *et al.* have also reported the development of a pressure shockwave that radially propagates towards outside [39]. It results in the vaporisation of the surrounding electrolyte and the expansion of a gas bubble. By using fast video imaging to follow the dynamic of bubbles created by discharge in dielectric liquids and, by applying the Rayleigh-Plesset's cavitation model, Hamdan *et al.* estimated the initial pressure inside the bubble at several hundreds of bars [40, 41]. More recently, by investigating individual discharges during plasma electrolytic oxidation, Throughton *et al.* estimated the pressure in the gas bubble at about 2.5 bars [39]. After the extinction of the micro-discharges, whose life-time is about 10 µs [9, 17, 33, 34, 37], the gas bubble continues its expansion through the cavity of the "pancake" structure as illustrated in Fig. 11c. Because of the pressure gradient between the pancake cavity filled with a gas phase ($P > P_{atm}$) and the electrolyte (P_{atm}), the molten part of the oxide is pushed out of the cavity of the "pancake" structure towards the electrolyte. The molten oxide can only leave through the narrow orifice located at the top of the "pancake" structure and gradually inflates similarly to a rubber balloon (Fig. 11d). In contact with the cooled electrolyte, the molten oxide is rapidly cooled at a cooling rate of ~ 10^7 $K.s^{-1}$ [12]. Under such a severe cooling condition, the oxide is quenched keeping a hollow spherical shape. Cracks appear at its surface

due to the volume retraction of the oxide during solidification (Fig. 11e).The solidified particle may then either remain attached at the pancake or be ejected into the electrolyte if the electrolyte turbulence is sufficiently strong or if other micro-discharges ignite in the “pancake” cavity (Fig. 11f).

5. Conclusions

The formation of particles during the PEO processing of aluminium and zirconium alloys was investigated. The microstructure of the particles was characterized at different scales, mainly by using transmission electron microscopy. Whatever the processed material, results show that particles exhibit the same morphology *i.e.* a hollow spherical shape with diameters in the range of 10 nm to 10 µm. They consist of polycrystalline metallic oxides *i.e* η- and α-alumina for the PEO of aluminium alloys and monoclinic zirconia for the zirconium alloy. Microstructure of the produced particles was then compared to the microstructure of the PEO coatings grown on the metallic substrates. A correlation was drawn between the microstructure of the particles and the typical “pancake”-like structure of the PEO coating. On this basis, a descriptive mechanism of the formation of these particles was suggested as follows: Ignition of a micro-discharge inside the “pancake” cavity induces the propagation of a pressure shockwave that pushes the molten oxide through the exit orifice of the pancake. Like a rubber balloon, the molten oxide forms a hollow sphere and is rapidly solidified by the surrounding electrolyte and ejected towards the electrolyte.

Acknowledgments

- This work was supported by the French Government through the program "Investissements d'avenir" operated by the French National Research Agency (ANR) and referenced to as ANR-11-LABX-0008-01 ('LabEx DAMAS').
- The authors would like to acknowledge contributions of the following:
  - P. Boulet and the competence cluster on X-ray diffraction (CC-Xγ) at Institut Jean Lamour for providing advices in XRD measurements and analyses.
  - S. Mathieu, E. Etienne and the competence cluster on electron microscopy (CC 3M) at Institut Jean Lamour for providing advices in SEM observations and EDX analyses.

Data availability

The data that support the findings of this study are available upon reasonable request addressed to the corresponding author.

Contribution of each author

J. Martin and G. Henrion conceptualized the goal of this research work.

G. Henrion, J. Martin and V. Ntomprougkidis conceived the PEO experimental rigs.

P. Haraux and J. Martin performed most of the PEO experiments.

P. Haraux and J. Martin performed all the SEM, XRD and EDX analysis.

S. Migot performed FIB milling of the particles.

S. Bruyère performed TEM and STEM/EDX observations and measurements.

J. Martin, V. Ntomprougkidis and P. Haraux prepared the manuscript.

J. Martin and G. Henrion supervised the whole work.

All the authors analysed the results and reviewed the manuscript.

Additional information

The authors declare no competing financial interests.

List of references

[1] Gh. Barati Darband, M. Aliofkhazraei, P. Hamghalam, N. Valizade, Plasma electrolytic oxidation of magnesium and its alloys: Mechanism, properties and applications, J. Magnesium Alloy. 5 (2017) 74-132.

[2] Y. L. Cheng, J. Cao, M. Mao, H. Xie, P. Skeldon, Key factors determining the development of two morphologies of plasma electrolytic coatings on an Al-Cu-Li alloy in aluminate electrolytes. Surf. Coat. Technol. 291 (2016) 239-249.

[3] Y.L. Cheng, J. Cao, Z. Peng, Q. Wang, E. Matykina, P. Skeldon, G.E. Thompson. Wear resistant coatings formed on Zircaloy-2 by plasma electrolytic oxidation in sodium aluminate electrolytes. Electrochim. Acta 116 (2014) 453-466.

[4] A. Mathis, E. Rocca, D. Veys-Renaux, J. Tardelli, Electrochemical behaviour of titanium in KOH at high potential, Electrochim. Acta 202 (2016) 253-261.

[5] A.L. Yerokhin, X. Nie, A. Leyland, A. Matthews, S.J. Dowey, Plasma electrolysis for surface engineering, Surf. Coat. Technol. 122 (1999) 73–93.

[6] P. Gupta, G. Tenhundfeld, E.O. Daigle, D. Ryabkov, Electrolytic plasma technology: Science and engineering - An overview, Surf. Coat. Technol. 201 (2007) 8746-8760.

[7] J.A. Curran, T.W. Clyne, Thermo-physical properties of plasma electrolytic oxide coatings on aluminium, Surf. Coat. Technol. 199 (2005) 168-176.

[8] A. Santos-Coquillat, M. Mohedano, E. Martinez-Campos, R. Arrabal, A. Pardo, E. Matykina, Bioactive multi-elemental PEO-coatings on titanium for dental implant applications, Mater. Sci. & Eng.: C 97 (2019) 738-752.

[9] E. Matykina, A. Berkani, P. Skeldon, G.E. Thompson, Real-time imaging of coating growth during plasma electrolytic oxidation of titanium, Electrochim. Acta 53 (2007) 1987-1994.

[10] F. Monfort, A. Berkani, E. Matykina, P. Skeldon, G.E. Thompson, H. Habazaki, K. Shimizu, Development of anodic coatings on aluminium under sparking conditions in silicate electrolyte, Corros. Sci. 49 (2007) 672-693.

[11] V. Dehnavi, X.Y. Liu, B.L. Luan, D.W. Shoesmith, S. Rohani, Phase transformation in plasma electrolytic oxidation on 6061 aluminium alloy, Surf. Coat. Technol. 251 (2014) 106-114.

[12] J. Martin, A. Nominé, V. Ntomprougkidis, S. Migot, S. Bruyère, F. Soldera, T. Belmonte, G. Henrion, Formation of a mestastable nanostructured mullite during Plasma Electrolytic Oxidation of aluminium in "soft" regime condition, Mater. Design 180 (2019) 107977.

[13] A.L. Yerokhin, L.O. Snizhko, N.L. Gurevina, A. Leyland, A. Pilkington, A. Matthews, Discharge characterization in plasma electrolytic oxidation of aluminium, J. Phys. D: Appl. Phys. 36 (2003) 2110–2120.

[14] R.O. Hussein, X. Nie, D.O. Northwood, A. Yerokhin, A. Matthews, Spectroscopic study of electrolytic plasma and discharging behaviour during the plasma electrolytic oxidation (PEO) process, J. Phys. D: Appl. Phys. 43 (2010) 105203.

[15] J. Jovović, S. Stojadinović, N.M. Šišović, N. Konjević, Spectroscopic study of plasma during electrolytic oxidation of magnesium- and aluminium-alloy, J. Quant. Spectrosc. Rad. Trans. 113 (2012) 1928‑1937.

[16] S. Stojadinović, R. Vasilić, M. Perić, Investigation of plasma electrolytic oxidation on valve metals by means of molecular spectroscopy – a review, RSC Adv. 4 (2014) 25759-25789.

[17] T.W. Clyne, S.C. Troughton, A review of recent work on discharge characteristics during plasma electrolytic oxidation of various metals, Int. Mater. Rev. 64 (2019) 127-162.

[18] T. Zhan, W. Tu, Y. Cheng, J. Han, B. Su, Y. Cheng, The synthesis of micro and nano WO_3 powders under the sparks of plasma electrolytic oxidation of Al in a tungstate electrolyte, Ceram. Int. 44 (2018) 10402-10411.

[19] A. Allagui, R. Wüthrich, Gas film formation time and gas film lifetime during electrochemical discharge phenomenon, Electrochim. Acta 54 (2009) 5336-5343.

[20] A. Gromov, A. Nalivaiko, T. Fehn, D.P.M. Yahya, A. Osipenkova, A. Koleczko, S. Knapp, U. Teipel, Cathode plasma electrolysis in diluted potassium hydroxide solutions : Particles formation and energetic estimation, J. Electroanal. Chem. 844 (2019) 155-160.

[21] T. Abdul Kareem, A. Anu Kaliani, Glow discharge plasma electrolysis for nanoparticles synthesis, Ionics 18 (2012) 315-327.

[22] Y. Toriyabe, S. Watanabe, S. Yatsu, T. Shibayama, T. Mizuno, Controlled formation of metallic nanoballs during plasma electrolysis, Appl. Phys. Lett. 91 (2007) 041501.

[23] C. Liu, Q. Zhao, L. Wang, J. Zhang, Y. Tian, Y. Meng, One-step preparation of TiO_2 particles with controllable phase and morphology by plasma electrolysis, RSC Adv. 7 (2017) 39824-39832.

[24] Z. Wu, Z.K. Zhang, D.Z. Guo, Titanium dioxide nanospheres with wide spectral absorption prepared by low-voltage plasma electrolysis, J. Colloid Interf. Sci. 392 (2013) 463-464.

[25] Z.K. Zhang, M.L. Bai, D.Z. Guo, S.M. Hou, G.M. Zhang, Plasma-electrolysis synthesis of TiO_2 nano/microspheres with optical absorption extended into the infra-red region, Chem. Commun. 47 (2011) 8439.

[26] M. Bin Julaihi, P.N. Yuh Yek, S. Yatsu, S. Watanabe, formation of stainless steel nanoballs via submerged glow-discharge plasma and their microstructural analysis with evaluation of photocatalytic activity, ISIJ Inter. 58 (2018) 1162-1167.

[27] C. Liu, Y. Meng, W. Jia, W. Zhang, Q. Zhao, Y. Tian, Peanut shaped titanium oxide micro-particles achieved by cathode plasma electrolysis and their electrorheological characteristics, Smart Mater. Struct. 27 (2018) 115017.

[28] J. Wu, L. Fan, L. Dong, J. Deng, D. Li, Y. Zhang, W. Xue, Cathodic plasma electrolysis for preparation of diamond-like carbon particles in glycerol solution, Mater. Chem. Phys. 199 (2017) 289-294.

[29] A. Allagui, E. Baranova, R. Wüthrich, Synthesis of Ni and Pt nanomaterials by cathodic contact glow discharge electrolysis in acidic and alkaline media, Electrochim. Acta 93 (2013) 137-142.

[30] F. Jaspard-Mecuson, T. Czerwiec, G. Henrion, T. Belmonte, L. Dujardin, A. Viola, J. Beauvir, Tailored aluminium oxide layers by bipolar current adjustment in the Plasma Electrolytic Oxidation (PEO) process, Surf. Coat. Technol. 201 (2007) 8677–8682.

[31] A.B. Rogov, A. Yerokhin, A. Matthews, The role of cathodic current in Plasma Electrolytic Oxidation of aluminium: phenomenological concepts of the “soft sparking” mode, Langmuir 33 (2017) 11059-11069.

[32] D. S. Tsai, G. W. Chen, C. C. Chou, Probe the micro arc softening phenomenon with pulse transient analysis in plasma electrolytic oxidation, Surf. Coat. Technol. 357 (2019) 235-243.

[33] J. Martin, A. Nominé, F. Brochard, J.L. Briançon, C. Noël, T. Belmonte, T. Czerwiec, G. Henrion, Delay in micro-discharges appearance during PEO of Al: Evidence of a mechanism of charge accumulation at the electrolyte /oxide interface, Appl. Surf. Sci. 410 (2017) 29-41.

[34] J. Martin, A. Melhem, I. Shchedrina, T. Duchanoy, A. Nominé, G. Henrion, T. Czerwiec, T. Belmonte, Effects of electrical parameters on plasma electrolytic oxidation of aluminium, Surf. Coat. Technol. 221 (2013) 70-76.

[35] Y. Li, P. Kuai, P. Huo, C.-J. Liu, Fabrication of CuO nanofibers via the plasma decomposition of Cu(OH)2, Mater. Lett. 63 (2009) 188-190.

[36] D. Chen, G. Shen, K. Tang, Y. Qian, Large-scale synthesis of CuO shuttle-like crystals via a convenient hydrothermal decomposition route, J. Cryst. Growth 254 (2003) 225-228.

[37] A. Nominé, S.C. Troughton, A.V. Nomine, G. Henrion, T.W. Clyne, High speed video evidence for localised discharge cascades during plasma electrolytic oxidation, Surf. Coat. Technol. 269 (2015) 125–130.

[38] S.C. Troughton, A. Nominé, J. Dean, T.W. Clyne, Effect of individual discharge cascades on the microstructure of plasma electrolytic oxidation coatings, Appl. Surf. Sci. 389 (2016) 260–269.

[39] S.C. Troughton, A. Nominé, A.V. Nominé, G. Henrion, T.W. Clyne, Synchronised electrical monitoring and high-speed video of bubble growth associated with individual discharges during plasma electrolytic oxidation. Appl. Surf. Sci. 359 (2015) 405–411.

[40] A. Hamdan, C. Noel, F. Kosior, G. Henrion, T. Belmonte, Dynamics of bubbles created by plasma in heptane for micro-gap conditions, J. Acoust. Soc. Am. 134 (2013) 991-1000.

[41] A. Hamdan, I. Marinov, A. Rousseau, T. Belmonte, Time-resolved imaging of nanosecond-pulsed micro-discharges in heptane,J. Phys. D: Appl. Phys. 47 (2014) 055203-055211.

List of tables

Table 1: Chemical compositions of a 1050 aluminium alloy (noted Al-1050), a 2024 aluminium alloy (noted Al-2024) and a M5 zirconium alloy (noted Zr-M5).

	Elements	**Fe**	**Si**	**Zn**	**Cu, Mg, Mn, Ti**	**Al**
Al-1050	in wt.%	0.40	0.25	0.07	<0.05	Balance

	Elements	**Cu**	**Mg**	**Mn**	**Si, Fe, Zn, Cr, Ti**	**Al**
Al-2024	in wt.%	3.8 - 4.9	1.2 – 1.8	0.3 – 0.9	<0.5	Balance

	Elements	**Nb**	**O**	**Fe, S**	**Zr**
Zr-M5	in wt.%	1	0.14	<0.05	Balance

Table 2: Elemental composition of the particles produced during the PEO process of Al-1050, Al-2024 and Zr-M5 alloys.

	Al	**Zr**	**O**	**Cu**	**Ti**	**C**
Spot 4[*] (in at.%)	38.4	-	58.4	3.2	-	-
Spot 5 (in at.%)	1.1	-	52.3	43.5	-	3.1
Spot 6 (in at.%)	41.3	-	57.7	-	1	-
Spot 7 (in at.%)			65.7	-	-	-

[*] *From STEM/EDX analysis performed in regions reported in Fig.7.*

List of figures

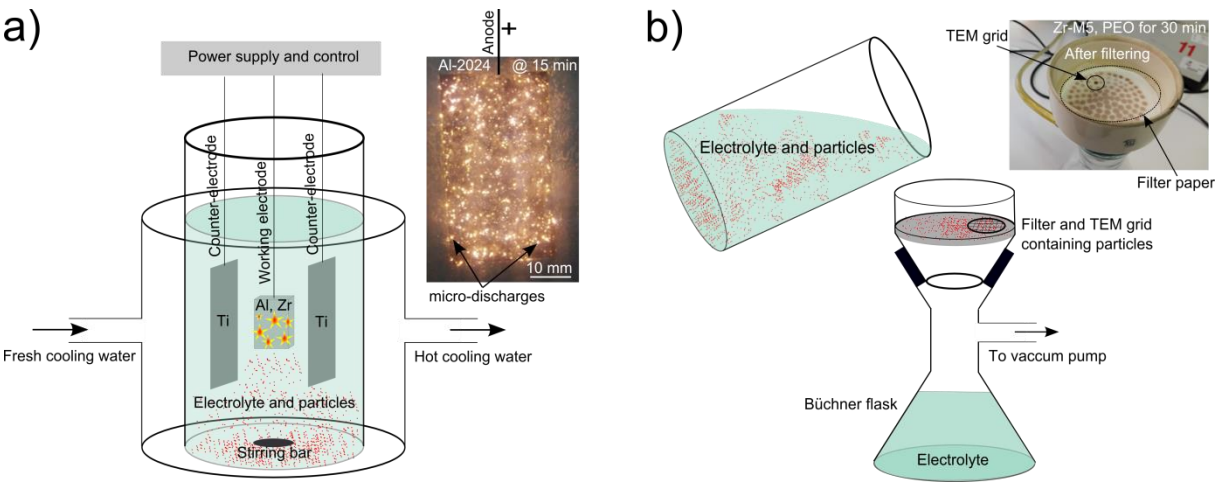

Fig. 1: Schematic view of the experimental procedure that allows **a)** producing particles using the PEO process (picture of a 2024 aluminium alloy during PEO at 15 min processing time) and **b)** collecting particles using the Büchner filtering method (picture of the filter paper and the TEM grid after filtering).

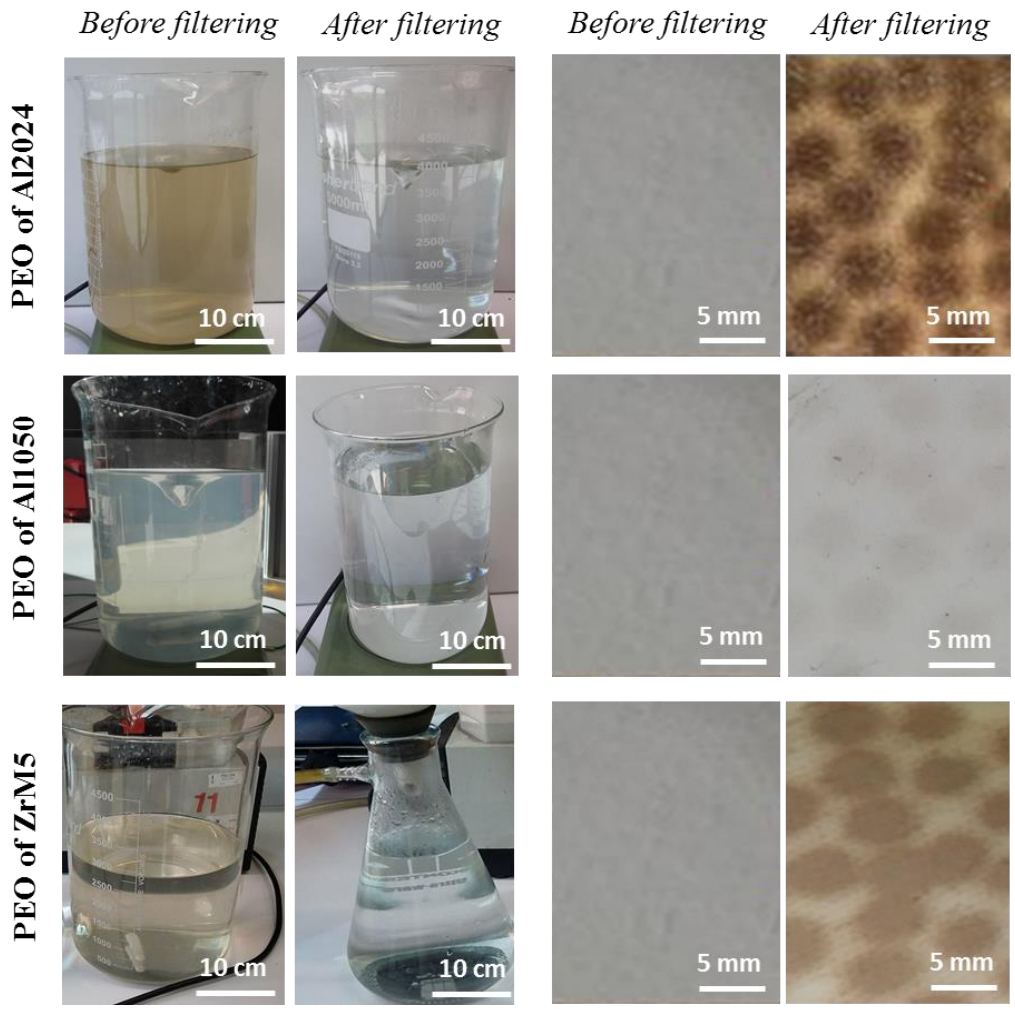

Figure 2: Visual aspect of the electrolytes and the filter papers (before and after filtering) for the PEO process of Al-2024, Al-1050 and Zr-M5 alloys.

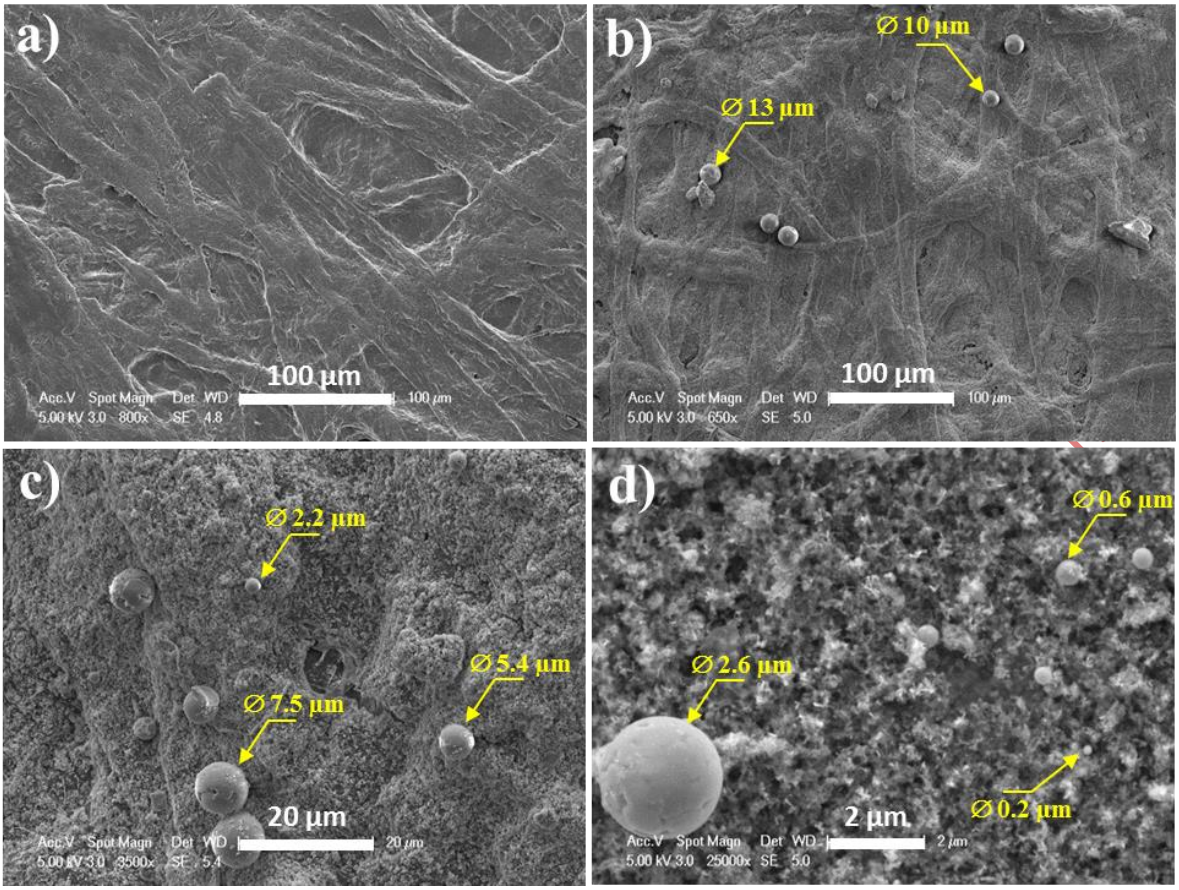

Figure 3: SEM micrographs of the filter paper recorded at different magnifications **a)** before filtering and **b)**, **c)**, **d)** after filtering in the case of the PEO process of an Al-2024 aluminium sample.

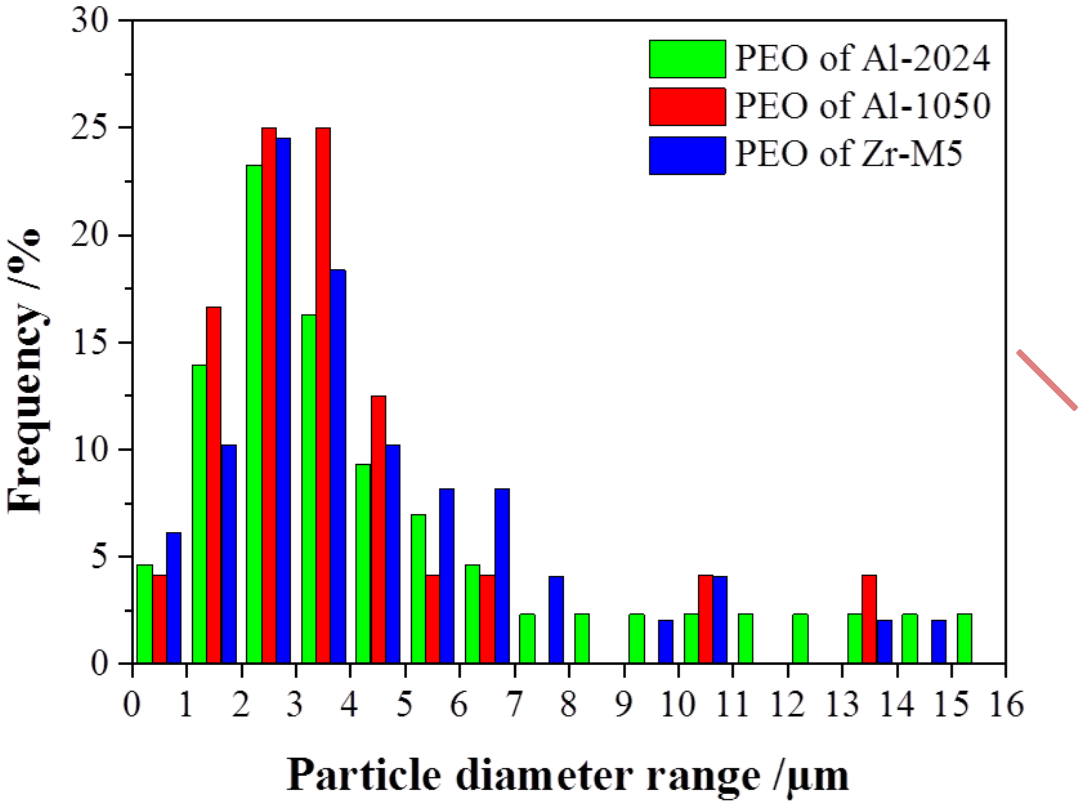

Figure 4: Size distribution of the spherical particles observed on the filter paper by SEM and TEM after the PEO process of Al-1050, Al-2024 and Zr-M5 alloys.

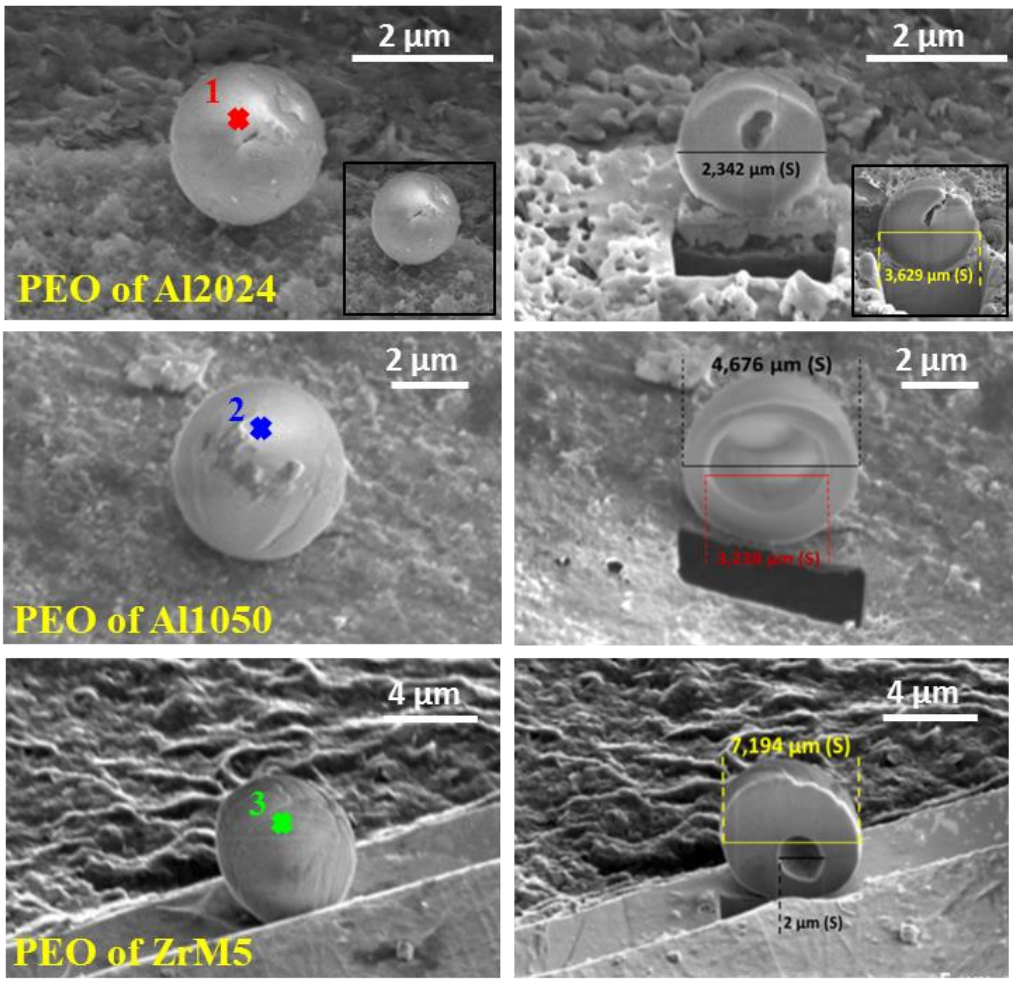

Figure 5: SEM micrographs of the particles (before and after FIB milling) produced during the PEO process of Al-1050, Al-2024 and Zr-M5 alloys. Coloured spots indicate locations of EDX measurements shown in Fig. 6.

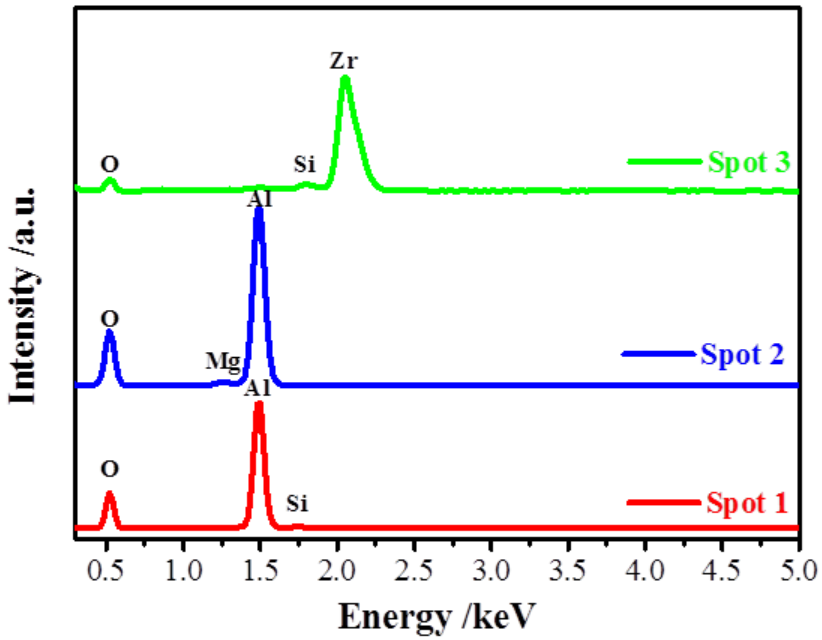

Figure 6: EDX spectra recorded on the particles produced during the PEO process of Al-1050, Al-2024 and Zr-M5 alloys. Location of spots 1, 2 and 3 are given in SEM micrographs in Fig.

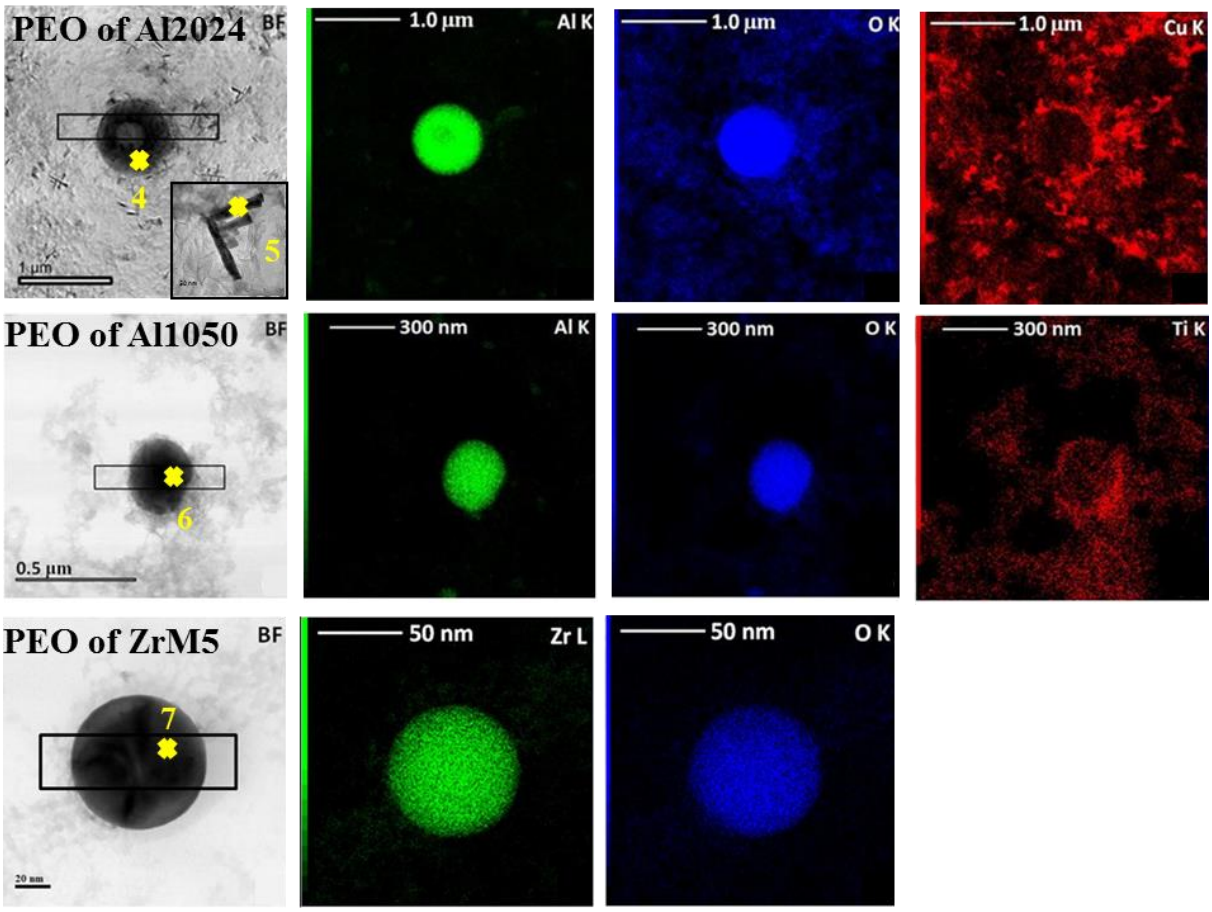

Figure 7: Bright-field STEM (BF-STEM) micrographs recorded on the particles produced during the PEO process of Al-1050, Al-2024 and Zr-M5 alloys and the associated STEM/EDX elemental map distributions.

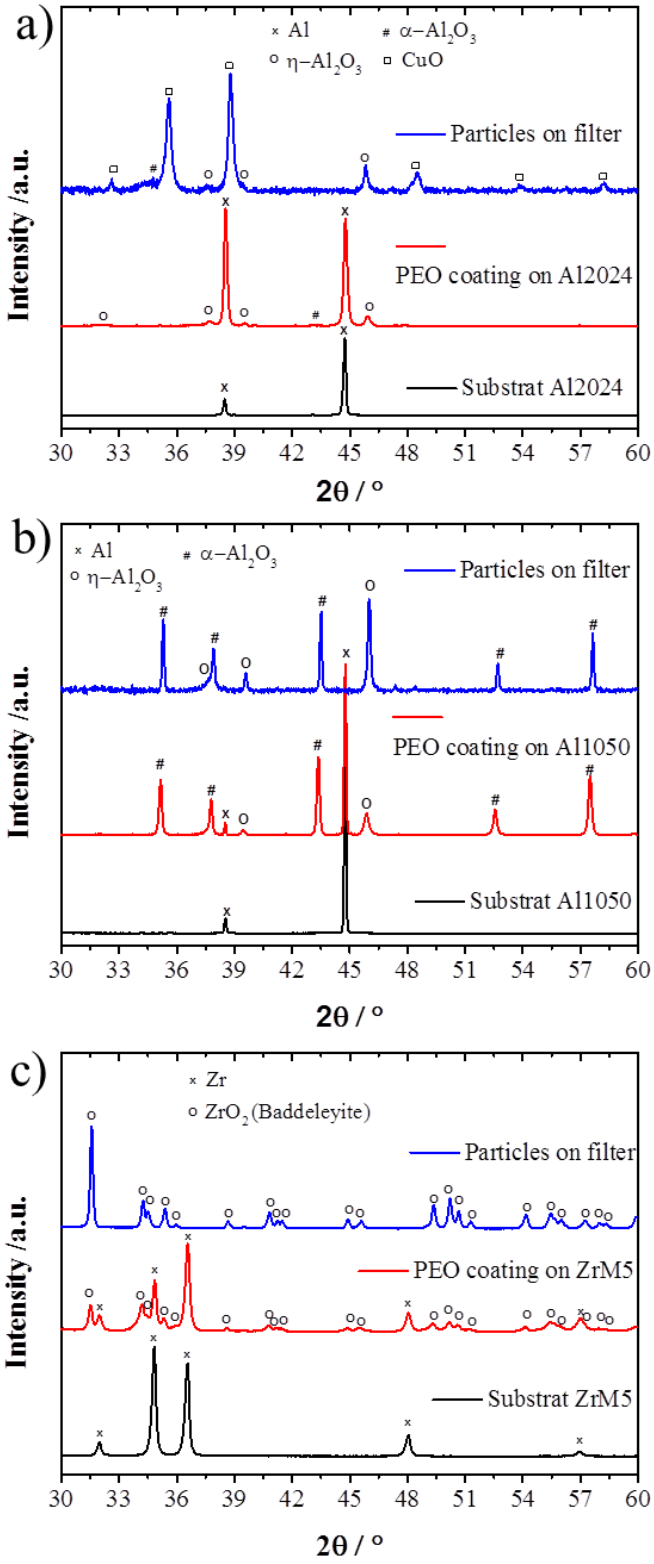

Figure 8: XRD patterns of the metallic substrate, the PEO oxide coating and the filter paper (after filtering the electrolyte) in the case of **a)** Al-1050, **b)** Al-2024 and **c)** Zr-M5 alloys.

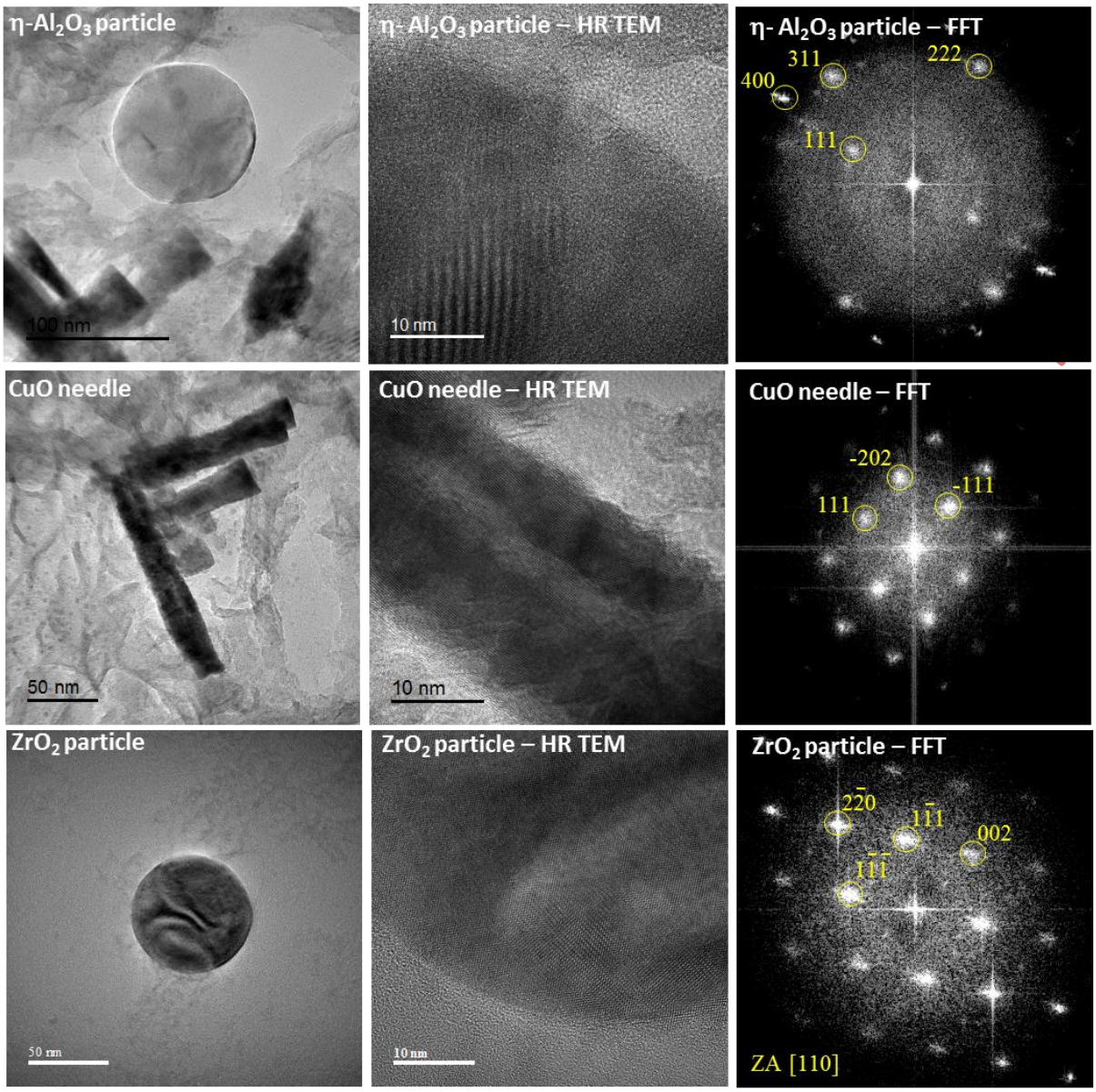

Figure 9: Bright-field TEM micrographs, high-resolution TEM micrographs and the associated FFT patterns recorded on the particles produced during the PEO process of Al-2024 and Zr-M5 alloys.

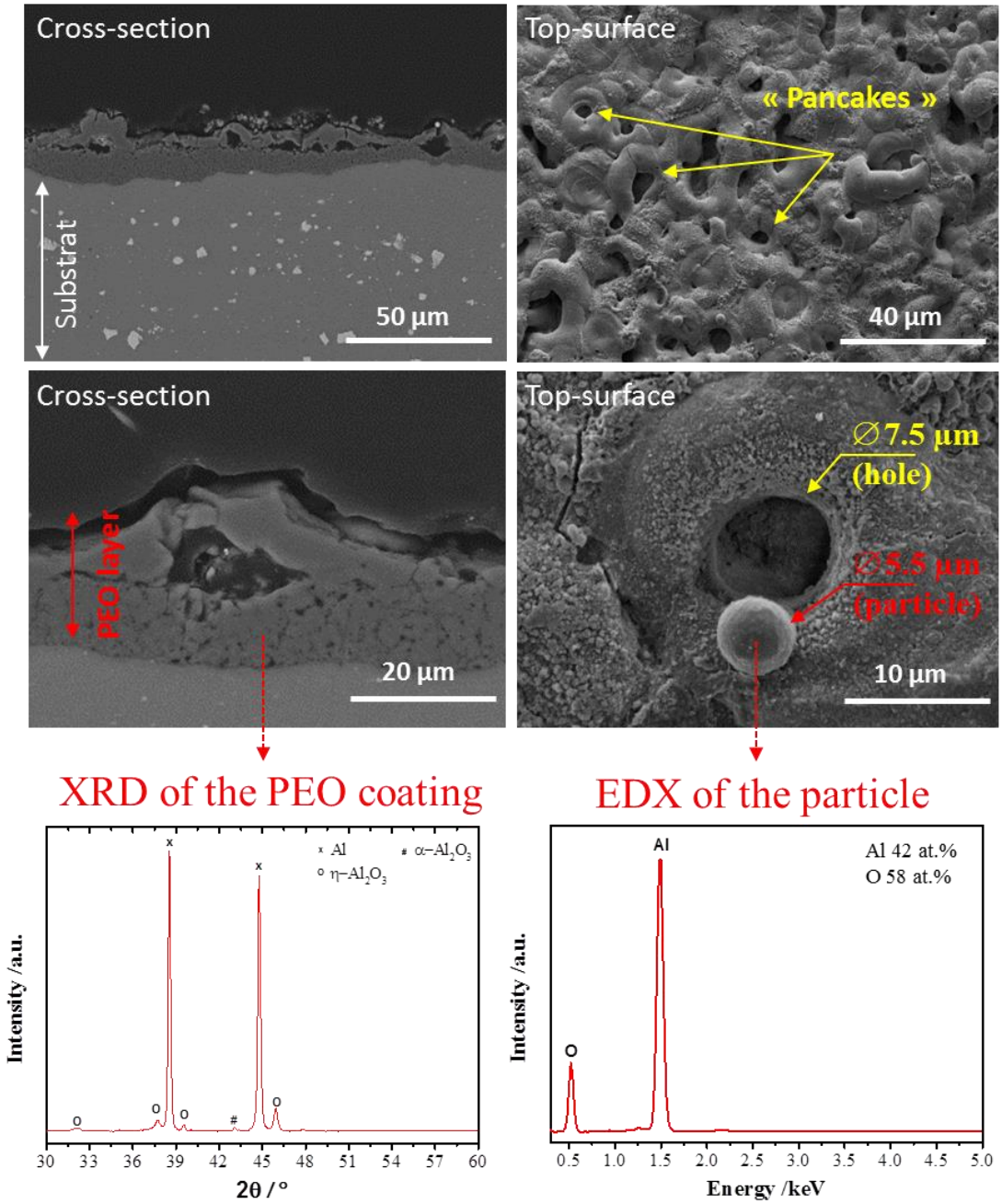

Figure 10: Cross-sectional and top-view SEM micrographs of the PEO coating elaborated on the copper-alloyed 2024 aluminium. XRD pattern of the elaborated PEO coating and EDX spectrum specifically recorded on a spherical particle attached on the top-surface of the PEO coating.

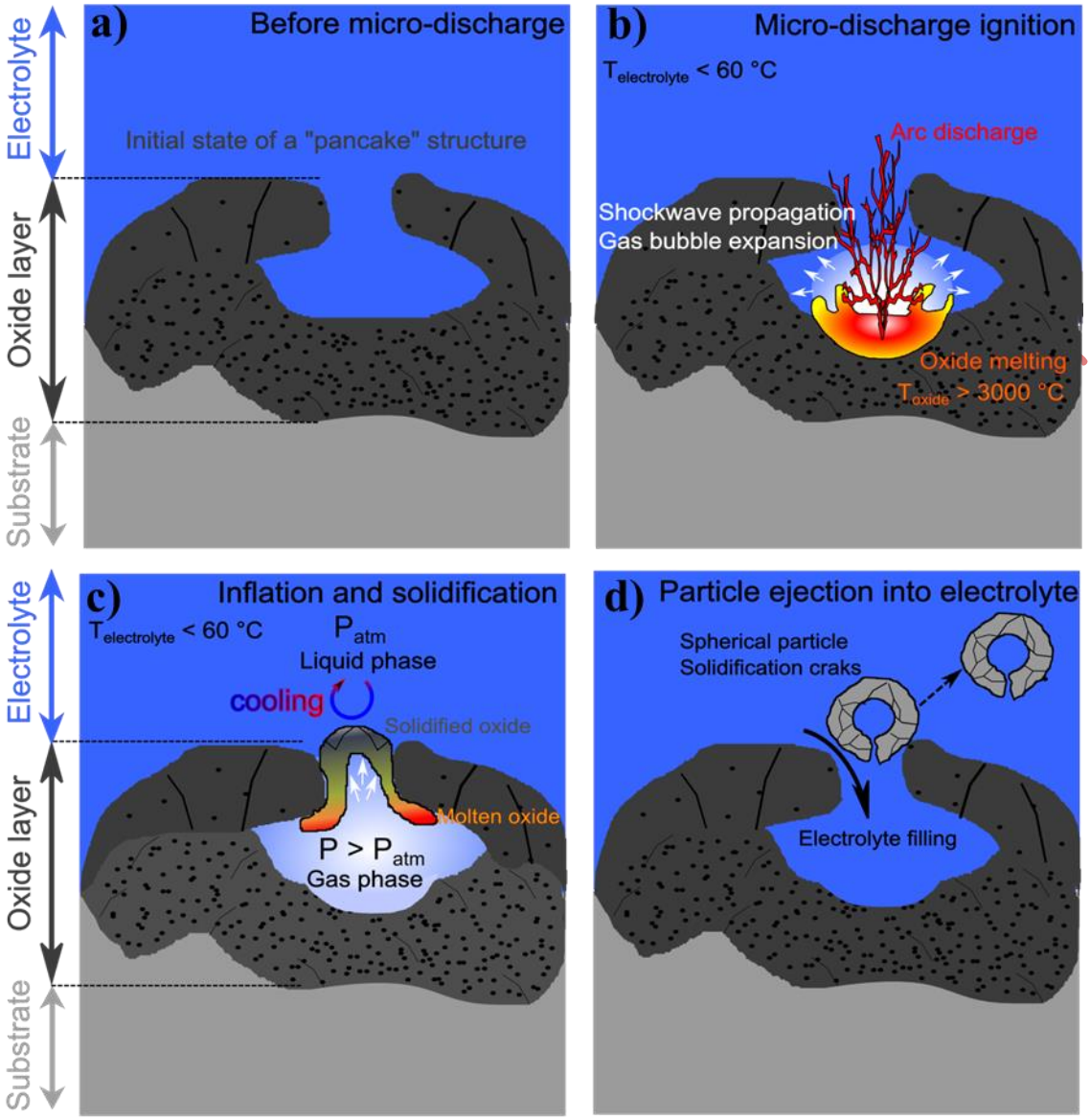

Figure 11: Schematic description of the formation mechanism of the metal oxide particles during the PEO process of aluminium and zirconium alloys. **a)** "Pancake" structure before the appearance of a micro-discharge. **b)** Ignition of a micro-discharge inside the "pancake" cavity resulting in the melting of the pre-existing oxide and the propagation of a pressure shockwave. **c)** The molten oxide is pushed towards the electrolyte under a pressure gradient between the "pancake" cavity ($P > P_{atm}$) and the electrolyte (P_{atm}) and inflates through the open hole of the "pancake" structure. A spherical particle is formed and rapidly quenched by the surrounding cooled electrolyte. **d)** Solidification cracks appear due to volume retraction and the solidified particle is ejected into the electrolyte.